

Structural anomalies for a three dimensional isotropic core-softened potential

Alan Barros de Oliveira

*Instituto de Física, Universidade Federal do Rio Grande do Sul,
Caixa Postal 15051, 91501-970, Porto Alegre, RS, BRAZIL.*

Paulo A. Netz

*Instituto de Química, Universidade Federal do Rio Grande do Sul,
91501-970, Porto Alegre, RS, BRAZIL.*

Thiago Colla and Marcia C. Barbosa

*Instituto de Física, Universidade Federal do Rio Grande do Sul,
Caixa Postal 15051, 91501-970, Porto Alegre, RS, BRAZIL*

(Dated: September 12, 2018)

Abstract

Using molecular dynamics simulations we investigate the structure of a system of particles interacting through a continuous core-softened interparticle potential. We found for the translational order parameter, t , a local maximum at a density ρ_{t-max} and a local minimum at $\rho_{t-min} > \rho_{t-max}$. Between ρ_{t-max} and ρ_{t-min} , the t parameter anomalously decreases upon increasing pressure. For the orientational order parameter, Q_6 , was observed a maximum at a density $\rho_{t-max} < \rho_{Qmax} < \rho_{t-min}$. For densities between ρ_{Qmax} and ρ_{t-min} , both the translational (t) and orientational (Q_6) order parameters have anomalous behavior. We know that this system also exhibits density and diffusion anomaly. We found that the region in the pressure-temperature phase-diagram of the structural anomaly englobes the region of the diffusion anomaly that is larger than the region limited by the temperature of maximum density. This cascade of anomalies (structural, dynamic and thermodynamic) for our model has the same hierarchy of that one observed for the SPC/E water.

PACS numbers: 64.70.Pf, 82.70.Dd, 83.10.Rs, 61.20.Ja

I. INTRODUCTION

Water is the most important substance for life: It cools, carries, stabilizes, reacts, lubricates, dilutes, and much more. Despite of this, many of its characteristics are not well understood. While most liquids contract upon cooling, water expands below $T = 4^{\circ}\text{C}$ at ambient pressure¹. This is known as the density anomaly of water. Heating the water from $T = 0^{\circ}\text{C}$ up to $T = 4^{\circ}\text{C}$ a competition between open low density and a closed high density structure takes place. The gain of thermal energy breaks a considerable number of hydrogen bonds what leads the open low density structure to become unstable in relation to the closed high density structure. So, the system contracts.

Density anomaly is not the only one, far from it, the literature reports forty-one anomalies for water². Not only the thermodynamics of water is anomalous, but also its dynamics. Commonly the materials diffusivity decreases with increasing pressure. Liquid water has an opposite behavior in a large region of the phase diagram^{3,4,5,6,7,8,9,10,11}. Increase in pressure disturbs the structure by inclusion of interstitial molecules that share an hydrogen bond with another one. As a result, the bond is weakened and the molecule is free to move. The shared bond breaks and the molecule by means of a small rotation, connects to another molecule enabling the translational diffusion³.

Water is not an isolated case. There are other examples of tetrahedrally bonded molecular liquids such as silica and silicon^{12,13} that exhibit thermodynamic and dynamic anomalies. Thermodynamic anomalies were also found in liquid metals¹⁴ and graphite¹⁵. Unfortunately, a closed theory giving the relation between the form of the interaction potential and the presence of the anomalies is still missing.

It is reasonable to think that the structure and anomalies are deeply related. Establishing the connection between structure and the thermodynamic and dynamic behavior of water is a fundamental step towards understanding the source of the anomalies. At this point a question emerges: how can we define (measure) structure in liquids? Errington and Debenedetti⁸ proposed two simple metrics: a translational order parameter¹⁶, t , that measures the tendency of pairs of molecules to adopt preferential separations, and the orientational order parameter^{8,17}, q , quantifying the extend to which a molecule and its four nearest neighbors assume a tetrahedral arrangement. For other crystal configurations one may use the orientational order parameter introduced by Steinhardt *et al.*¹⁸, Q_6 , which depends on the number

of nearest neighbors taken into account for each molecule. For a completely uncorrelated system (ideal gas) both t and q must be zero and Q_6 , is equal to one over the square of the number of neighbors. For a crystal, t , q and Q_6 are large. Torquato *et al.*¹⁹ introduced a systematic way to study the structural order in liquids mapping state points into the $t - q$ plane. They refer to it as an order map. Errington and Debenedetti used the order map to investigate structural order in simple point charge/extended (SPC/E) water⁸.

For normal liquids, t and q increase upon compression, because the system tends to be more structured. It was found that in SPC/E water both t and q decrease upon compression in a certain region of the pressure-temperature (P-T) phase diagram⁸. This region is referred as the region of structural anomalies. Errington and Debenedetti showed also that, inside the structurally anomalous region, all the paths formed by the (t, q) points collapse into a single line. This means that the translational order parameter, t , and the orientational order parameter, q , are coupled. Outside the structurally anomalous region the states points in the order map define a two-dimensional region, meaning that the parameters t and q are independent.

Performing molecular dynamics simulations, Errington and Debenedetti⁸ and Netz *et al.*⁹ showed that in SPC/E water the thermodynamic and dynamic anomalies form nested domes in the P-T phase-diagram, where the diffusion anomaly lies outside the density anomaly. Additionally, Errington and Debenedetti showed that the structurally anomalous region englobes the diffusion and density anomalies regions.

Several models of water for computer simulations have been proposed²⁰, with three, four or five localized partial charges, some of them having Lennard-Jones interaction centers in the oxygens and hydrogens, others only in the oxygens. A considerable number of these approaches reproduce many anomalies present in liquid water. However, these models are complicated, what makes difficult to understand the physics behind the anomalies. In this sense, isotropic models are the simplest framework to understand the physics of liquid state anomalies. Moreover, the use of an effective potential is particularly suitable for extending our conclusions for more complex fluids. From the desire of constructing a simple two-body isotropic potential, capable of describing water-like anomalies, a number of models in which single component systems of particles interact via core-softened (CS) potentials²¹ have been proposed. They possess a repulsive core that exhibits a region of softening where the slope changes dramatically. This region can be a shoulder or a

ramp^{22,23,24,25,26,27,28,29,30,31,32,33,34,35,36,37,38,39,40,41,42,43}.

In the shoulder case, the potential consists of a hard core, a repulsive shoulder and, in some cases, an attractive square well^{22,23,24,25,26,27,28,29,30,31,32,33,34,37}. The potential has a change in the slope at short-ranged distances. In two dimensions, such potentials have thermodynamic and diffusion anomalies. In three dimensions, no dynamic and thermodynamic anomalies were reported^{24,25,26,27,31,32}.

In the ramp case, the interaction potential has two competing equilibrium distances, defined by a repulsive ramp^{36,37,38,40,41,42,43}. In some cases an attractive part is included^{36,37,42}. In two dimensions, there are thermodynamic anomalies in such potentials. In three dimensions, these potentials exhibit not only thermodynamic anomalies, but also dynamic and structural anomalies^{38,40,41,43}.

Notwithstanding the progresses described above, a model in which both the potential and the force are continuous functions and that exhibits all the thermodynamic and dynamic anomalies like the ones present in water is still missing. In this paper, we check if a ramp-like potential previously studied by us⁴³ has not only density and diffusion anomalies, but also structural anomalies. We will verify if the region in the pressure-temperature phase-diagram of thermodynamic and dynamic anomalies are inside the region of structural anomalies as in SPC/E water⁸. The hierarchy between the anomalies in such simple model is an important step in order to understand the mechanism of the anomalies.

The reminder of this paper goes as follows. In sec. II the model is introduced; in sec. III the methods for calculating structural order in liquids are presented. Results for the structural anomalies and the order map obtained from molecular dynamics simulations are shown in sec. IV. Conclusions about the relation between the locus of the thermodynamic, dynamic and structural anomalies and about the order map are presented in sec. V.

II. THE MODEL

The model we study consists of a system of N particles of diameter σ interacting through an isotropic effective potential given by

$$U^*(r) = 4 \left[\left(\frac{\sigma}{r} \right)^{12} - \left(\frac{\sigma}{r} \right)^6 \right] + a \exp \left[-\frac{1}{c^2} \left(\frac{r - r_0}{\sigma} \right)^2 \right], \quad (1)$$

where $U^*(r) = U(r)/\epsilon$. The first term of Eq. (1) is a Lennard-Jones potential of well depth ϵ and the second term is a Gaussian centered on radius $r = r_0$ with height a and width c . Depending on the choice of the values of a , r_0 and c , this potential assumes several shapes ranging from a deep double well potential^{44,45,46} to a repulsive shoulder³⁶.

Recently, using molecular dynamics simulations and integral equations theory, we have studied the potential Eq. (1) setting $a = 5$, $r_0/\sigma = 0.7$ and $c = 1$ (see Fig. 1)⁴³. Here, we use the same parameters (as in the previous⁴³). It is interesting to note that close to the core ($r/\sigma \approx 1$) this potential experiences an unusual change of slope, weakening the repulsive force between the particles.

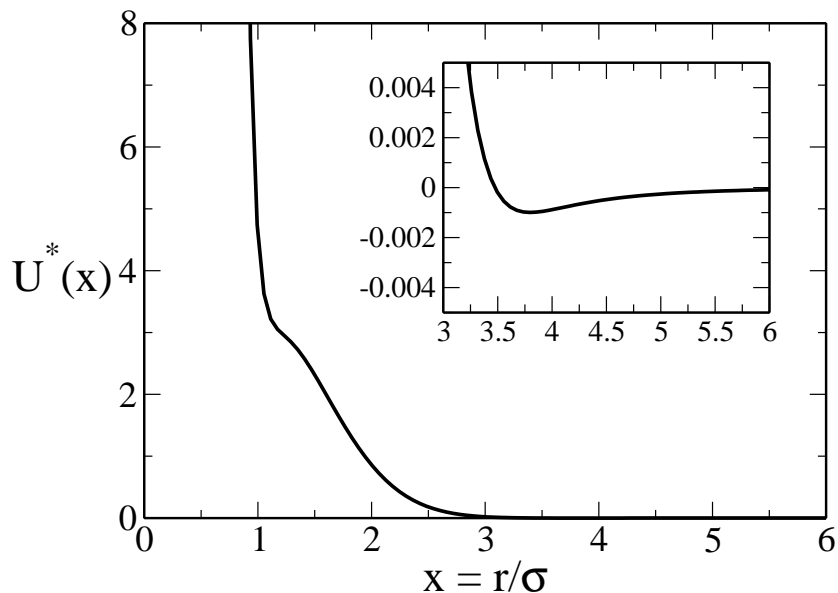


FIG. 1: Interaction potential eq. (1) with parameters $a = 5$, $r_0/\sigma = 0.7$ and $c = 1$, in reduced units. The inset shows a zoom in the very small attractive part of the potential.

III. THE METHODS

A. Translational order parameter

The translational order parameter of a system of particles of density $\rho = N/V$, where N is the number of particles and V is the volume of the system, is defined as^{8,13,16},

$$t \equiv \int_0^{\xi_c} |g(\xi) - 1| d\xi, \quad (2)$$

where $\xi \equiv r\rho^{1/3}$ is the interparticle distance r divided by the mean separation between pairs of particles $\rho^{-1/3}$. $g(\xi)$ is the radial distribution function, where g is proportional to the probability to find a particle at a distance ξ to another particle placed at the origin. ξ_c is a cut-off distance. In this work, we use⁴⁷ $\xi_c = \rho^{1/3}L/2$, where $L = V^{1/3}$. For a completely uncorrelated system (ideal gas) $g = 1$ and t vanishes. In a crystal, a translational long-order ($g \neq 1$) persists over long distances making t large.

B. Orientational order parameter

For the orientational order parameter introduced by Steinhardt *et al.*¹⁸, we follow the strategy introduced by Yan *et al.*⁴⁰. We define k vectors, \mathbf{r}_{ij} , connecting the particle i with its k nearest neighbors j . Each vector \mathbf{r}_{ij} is a "bond". A polar (ϕ_{ij}) and azimuthal (θ_{ij}) angles with reference to an arbitrary axis may be associated to each bond r_{ij} and the spherical harmonics $Y_{lm}(\theta_{ij}, \phi_{ij})$ may be calculated. After computing the average of $Y_{lm}(\theta_{ij}, \phi_{ij})$ over the k bonds, namely,

$$\langle Y_{lm}^i \rangle = \frac{1}{k} \sum_{j=1}^k Y_{lm}(\theta_{ij}, \phi_{ij}), \quad (3)$$

one can evaluate the orientational order parameter^{8,13,16,19,48,49} associated to each particle i ,

$$Q_l^i = \left[\frac{4\pi}{2\ell+1} \sum_{m=-\ell}^{m=\ell} |\langle Y_{lm}^i \rangle|^2 \right]^{1/2}. \quad (4)$$

For characterize the local order⁵⁰ of the system was used^{40,41}

$$Q_6 = \frac{1}{N} \sum_{i=1}^N Q_6^i, \quad (5)$$

that is the mean value of Q_6^i over all particles of the system. The Q_6 parameter assumes its maximum value for a perfect crystal and decreases as the system becomes less structured. For a completely uncorrelated system (ideal gas) $Q_6^{ig} = 1/\sqrt{k}$. For a crystal, the Q_6 value depends on the specific crystalline arrangement and the number of neighbors taken into account. For example, for the face centered cubic (fcc) with its twelve first neighbors ($k = 12$), we have $Q_6^{fcc} = 0.574$. For a body centered cubic (bcc), which have only eight nearest neighbors,

$Q_6^{bcc-8} = 0.628$. Note that if we include not eight, but fourteen neighbors for calculating Q_6^{bcc-k} , we have $Q_6^{bcc-14} = 0.510$.

For the potential given by the Eq. (1), the expected crystalline configuration at the ground state for low densities is the hexagonal close packing (hcp), which have twelve first neighbors (see sec. IV for more details). In this work we used $k = 12$ in the Eq. (3). For the hcp crystal, $Q_6^{hcp} = 0.484$.

IV. RESULTS FROM SIMULATIONS

We performed molecular dynamics (MD) simulations in the canonical ensemble using 500 particles in a cubic box with periodic boundary conditions, interacting with the potential Eq. (1). The parameters employed were $a = 5$, $r_0/\sigma = 0.7$, and $c = 1.0$. The cutoff radius was set to $3.5\sigma^{51}$. In order to keep fixed the temperature, the Nosé-Hoover⁵² thermostat was used with the coupling constant $q_{NH} = 2$. Pressure, temperature, and density are shown in dimensionless units,

$$P^* \equiv \frac{P\sigma^3}{\epsilon} \quad (6)$$

$$T^* \equiv \frac{k_B T}{\epsilon} \quad (7)$$

$$\rho^* \equiv \rho\sigma^3. \quad (8)$$

The translational and orientational order parameters were calculated over 1 000 000 steps MD simulations, previously equilibrated over 200 000 steps. For low temperatures ($T^* < 0.4$), additional simulations were carried out with equilibration over 500 000 steps, followed by 2 000 000 steps simulation run. The time step was 0.002 in reduced units.

For studying the crystalline structure of our model we consider the expected, following conformations for the ramp potential³⁶: simple cubic (sc), body centered cubic (bcc), face centered cubic (fcc), simple hexagonal (sh), hexagonal close packing (hcp), and the rhombohedral-60° (rh60). Perfect crystals with such conformations were constructed and the configurational energy per particle $u = U^*/N$ was calculated for each arrangement. In the canonical ensemble, the most stable crystal at the ground state is that one with lower u .

From the Fig. 2, we see that the hcp conformation is the more stable for densities $\rho^* \lesssim 0.107$ (see inset). The bcc conformation is the more stable one for $0.107 \lesssim \rho^* \lesssim 0.187$ (not shown).

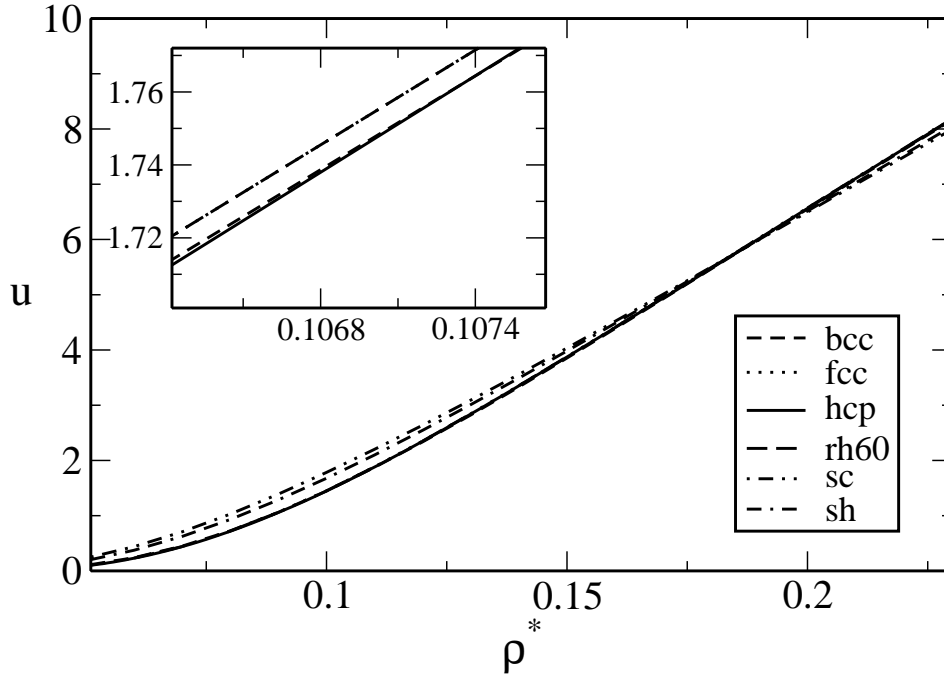


FIG. 2: The dimensionless configurational energy per particle for the several crystal structures considered: face centered cubic (fcc), body centered cubic (bcc), simple cubic (sc), simple hexagonal (sh), hexagonal closest packing (hcp), and rhombohedral-60° (rh60). We see that the hcp has the lower configuration energy per particle for densities $\rho^* \lesssim 0.107$ (see inset). Hence, the expected structure for our model at $T^* = 0$ is the hcp for $\rho^* \lesssim 0.107$. For $0.107 \lesssim \rho^* \lesssim 0.187$ the bcc phase has the lower configuration energy between those studied (not shown).

Studying the equation of state pressure against density for our model we found a monotonic behaviour for $P(\rho)$. Hence, an increase in pressure means increase in density as shown in Fig. 3.

Results for the translational order parameter for the liquid phase can be seen in the Fig. 4. While for a normal liquid t increases under compression, for our system this is the case only for high temperatures. For lower temperatures t presents a local maximum at a density ρ_{t-max} and a local minimum at a density $\rho_{t-min} > \rho_{t-max}$ for temperatures $T^* < 1.5$. Between ρ_{t-max} and ρ_{t-min} an unusual behavior for the translational order parameter is observed: An increase in density induces a decrease in translational order. This behavior

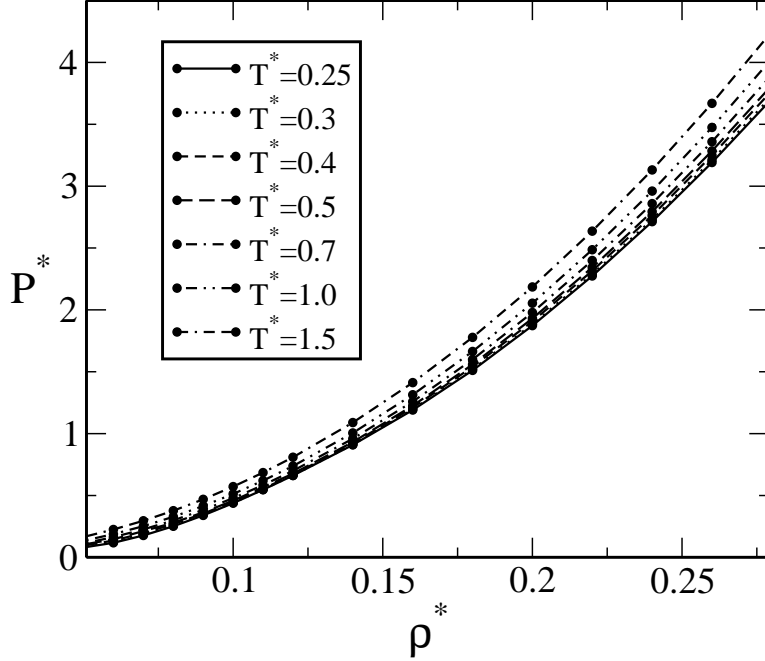


FIG. 3: The reduced pressure as a function of the reduced density. The seven isotherms show that the relation between P^* and ρ^* is monotonic.

can be understood analyzing the dependence of the radial distribution function (RDF) upon density [see Eq. (2)]. The (a), (b), and (c) arrows in the Fig. 4 correspond to the density range spanned by the Fig. 5(a), 5(b), and 5(c) respectively.

The Fig. 5 shows the RDF for $T^* = 0.25$ and several densities: (a) $\rho^* = 0.04, 0.06, 0.07$ and 0.08 ; (b) $\rho^* = 0.1, 0.11, 0.12, 0.14$, and 0.16 ; (c) $\rho^* = 0.18, 0.2, 0.22$, and 0.24 . The arrows indicate the directions of increasing ρ^* and the dashed line is the reduced interparticle potential shown in the Fig. 1 multiplied by a factor of 0.5 just for clarity. From Fig. 5(a) we see the growth of $g(r)$ at $r/\sigma \approx 2.5$ upon compression, causing an increasing of t over the range $0.04 \leq \rho^* \leq 0.08$. See the isotherm $T^* = 0.25$ at Fig. 4. In this range of densities the particles are repelled by the repulsive shoulder and the most probable separation is about 2.5 units (corresponding to the edge of the shoulder in the potential). We see that over the intermediate density range $0.08 < \rho^* < 0.18$, t decreases as the density increases. Looking at the Fig. 5(b) one can explain why this happens. Both an increase of $g(r)$ at $r/\sigma \approx 1.0$, approximating the RDF to 1 (what decreases $|g(r) - 1|$), and a decrease of $g(r)$ in the next peak (close to 2.5) upon compression, causes t to decrease. This new peak at about 1 unit

corresponds to the position of the hard-core part of the potential⁵³. Finally, t returns to increase upon compression for $\rho^* > 0.18$. The sharp growth of $g(r)$ at $r/\sigma \approx 1.0$ above the unity [see Fig.5(c)] underlies this behavior, indicating that all the particles are pushed together up to their hard-cores. This was the same behavior observed for the RDF of the ramp potential^{40,41}. Anomalous variations in t are absent for $T^* > 1.5$ because the thermal energy washes out the effect of the repulsive shoulder.

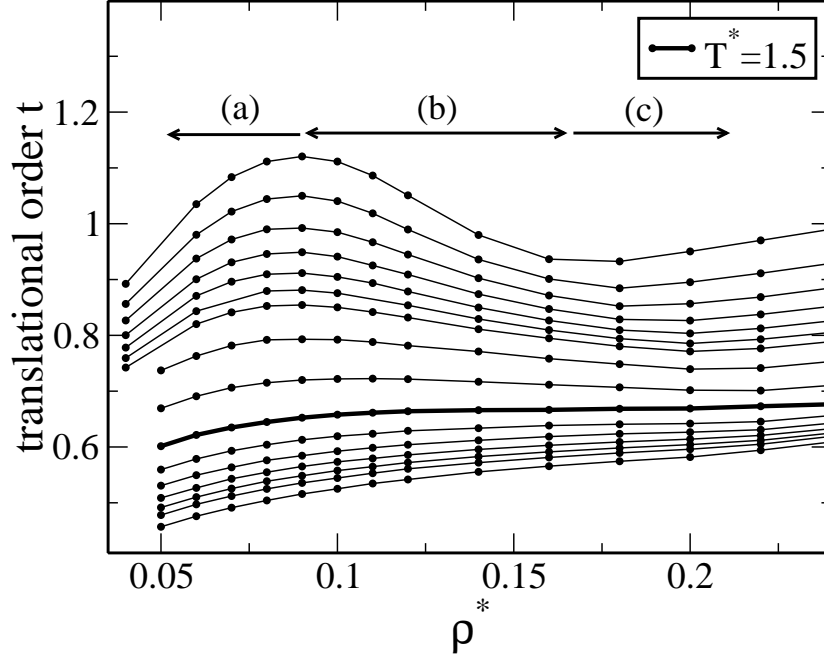


FIG. 4: The translational order parameter t as a function of the density ρ^* . From top to bottom, the sixteen isotherms are $T^* = 0.25, 0.30, 0.35, 0.40, 0.45, 0.50, 0.55, 0.70, 1.0, 1.5, 2.0, 2.5, 3.0, 3.5, 4.0,$ and 5.0 . The (a), (b), and (c) arrows corresponds to the density range spanned by the Fig. 5(a), 5(b), and 5(c) respectively. The bold line indicates the isotherm $T^* = 1.5$. For $T^* > 1.5$ no anomalous behavior is observed for t . The line connecting the points are just a guide for the eyes.

For a normal liquid, it is expected that the orientational order parameter, Q_6 , increases under compression. For our potential, however, a local maximum is detected for Q_6 at a density $\rho_{Q_{max}}$ in such a way that $\rho_{t-max} < \rho_{Q_{max}} < \rho_{t-min}$ (see figure 6). This means that for densities between $\rho_{Q_{max}}$ and ρ_{t-min} both the structural order parameters t and Q_6 have an anomalous behavior, since t and Q_6 decrease under increasing of pressure. We call this range of densities the structural anomaly domain.

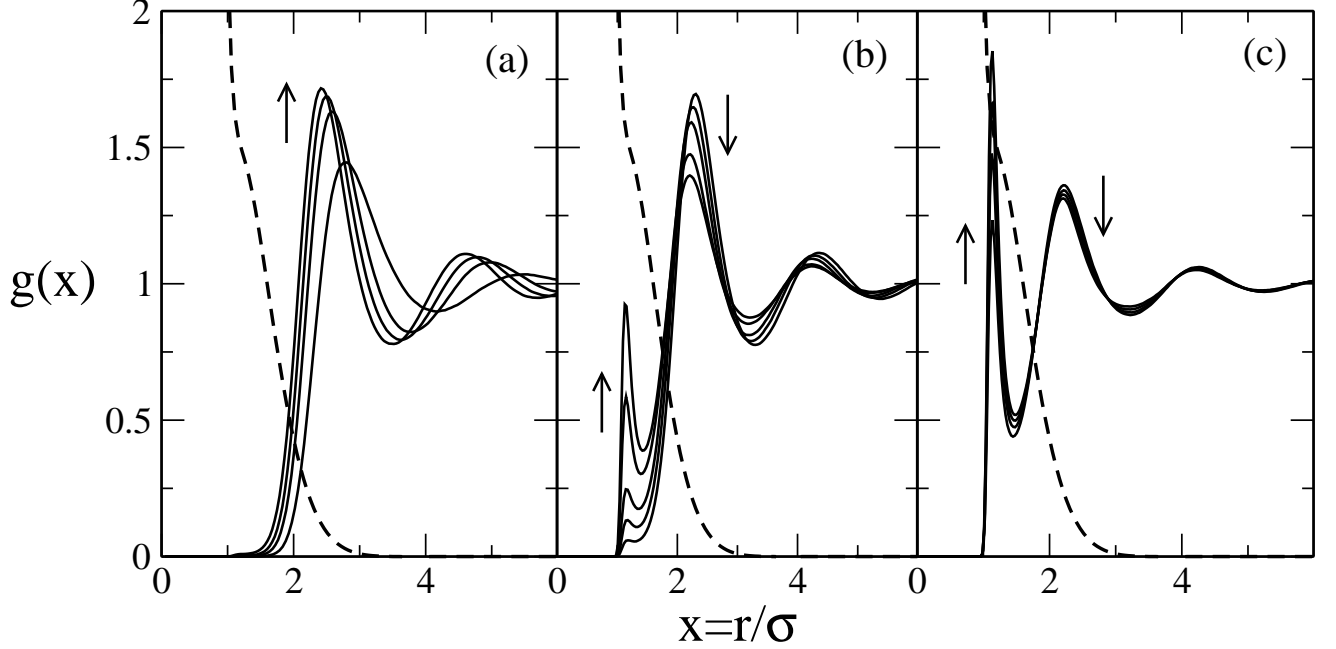


FIG. 5: The radial distribution functions for $T^* = 0.25$ and several densities: (a) $\rho^* = 0.04, 0.06, 0.07$, and 0.08 ; (b) $\rho^* = 0.10, 0.11, 0.12, 0.14$, and 0.16 ; (c) $\rho^* = 0.18, 0.20, 0.22$, and 0.24 . The arrows indicate the direction of increasing ρ^* . The dashed line is the reduced interparticle potential shown in the Fig. 1 multiplied by a factor of 0.5 just for clarity.

The relation between the several anomalies presented for this potential is shown in the Fig. 7. The temperature of maximum densities (TMD) and the diffusivity extrema (DE) lines were obtained from previous work⁴³. The TMD line indicates the region of thermodynamic anomaly region, inside which the density increases when the system is heated at constant pressure. The DE lines determinate the region of dynamic anomaly. Inside this region, diffusivity increases with increasing density. In this work we determinate additional three lines shown at Fig. 7: the curve of t maxima (C), the curve of Q_6 maxima (B), and the curve of t minima (A). We call the region between the curves A and B the structural anomalous region, inside which both the order parameters, t and Q_6 , become anomalous, namely, decrease with density. The curve B, composed by the Q_6 local maxima points, terminates at $T^* \approx 5.0$, not shown in the Fig. 7 for clarity. As the temperature T^* tends to 5.0, the densities for the Q_6 maxima loci tends to zero. For $T^* > 5.0$ we have studied the temperatures $T^* = 5.5, 6.0, 6.5, 7.0$, and 8.0 (not shown). For all these temperatures the same qualitative behavior for Q_6 was observed: The Q_6 parameter has local maxima at

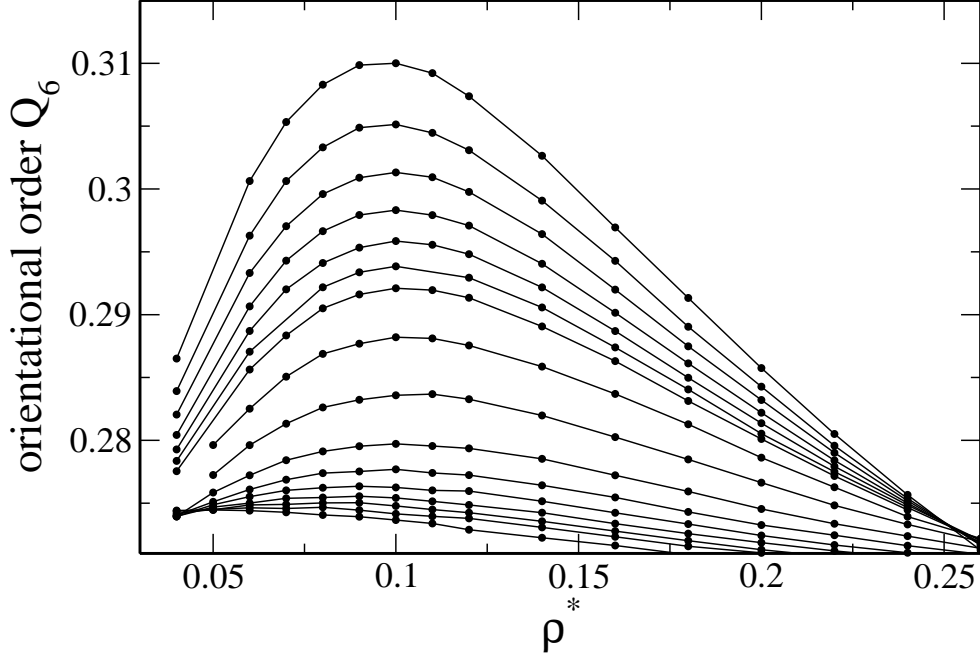


FIG. 6: The orientational order parameter Q_6 as a function of the density ρ^* . From top to bottom, the sixteen isotherms are $T^* = 0.25, 0.30, 0.35, 0.40, 0.45, 0.50, 0.55, 0.70, 1.0, 1.5, 2.0, 2.5, 3.0, 3.5, 4.0$, and 5.0 . For $5.0 < T^* < 8.0$ (not shown) the Q_6 local maximum points occur at $\rho^* = 0$ with a global minimum at $\rho^* \approx 0.3$. We do not study the cases where $T^* > 8.0$ (see the text for more details). The line connecting the points are just a guide for the eyes.

$\rho^* = 0$ and global minima at $\rho^* \approx 0.3$. The ratio between these extrema (local maxima and global minima) does not extrapolate 3.5% in any case. We do not simulate temperatures $T^* > 8.0$.

For the SPC/E water^{8,9}, the region of structural anomalies contains (inside) the region of dynamic anomalies, and the thermodynamic anomaly region lies inside this last one. For the silica, other tetrahedrally bonded molecular liquid, simulations show¹³ an inverse order between the structural and dynamic anomaly regions: The diffusion anomaly region englobes the structural anomaly region that englobes the thermodynamic anomaly region. For our model, we see a water-like cascade of anomaly regions similar to that found for the SPC/E water (see Fig. 7). This suggests that the role played by the structure in our potential, like in water, is determinant for giving rise to the other anomalies.

From the Fig. 2 its clear that for densities over 0.107 the hcp conformation is not the most

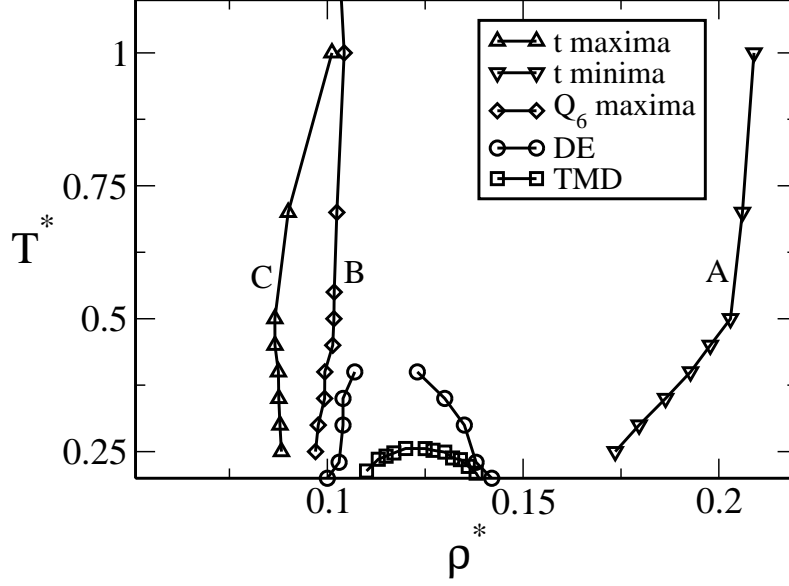


FIG. 7: The relationship between the several anomalies presented for our model. The curve B ends at $T^* \approx 5.0$ and it is not entirely shown for clarity. See the text for more details. Between the Q_6 maxima line (curve B) and t minima line (curve A) *both* the translational and orientational order parameters t and Q_6 become anomalous, namely, decrease with density. This region we call structural anomaly region. The diffusion extrema (DE) lines enclose the region inside which the diffusion decreases with density – the dynamic anomaly region. The temperature of maximum density (TMD) line englobes the region that density anomaly appears. Both the DE and TMD lines were obtained from previous work⁴³. These cascade of anomalies presents the same hierarchy as observed for the SPC/E water^{8,9}.

stable one between those studied. The bcc configuration becomes the expected crystalline arrangement for densities $0.107 \lesssim \rho^* \lesssim 0.187$. Hence, the calculation of the Q_6 parameter was repeated using eight first neighbors ($k = 8$) in the Eq. (3). For this new calculation, the entire curve B in the Fig. 7 is shifted approximately 13% (not shown) in the direction of lower densities, crossing the curve C. In this new scenario, the structural anomaly region now lies between the curves C and A, region in which both Q_6 and t decrease upon compression. Despite of this change, the whole qualitatively result is not modified, once the structural anomaly region remains outside the dynamic and thermodynamic regions.

As discussed in the introduction, the convenient orientational order parameter for tetrahedral liquids^{8,13} is q . It was reported that for SPC/E water the isothermal paths in a $t - q$

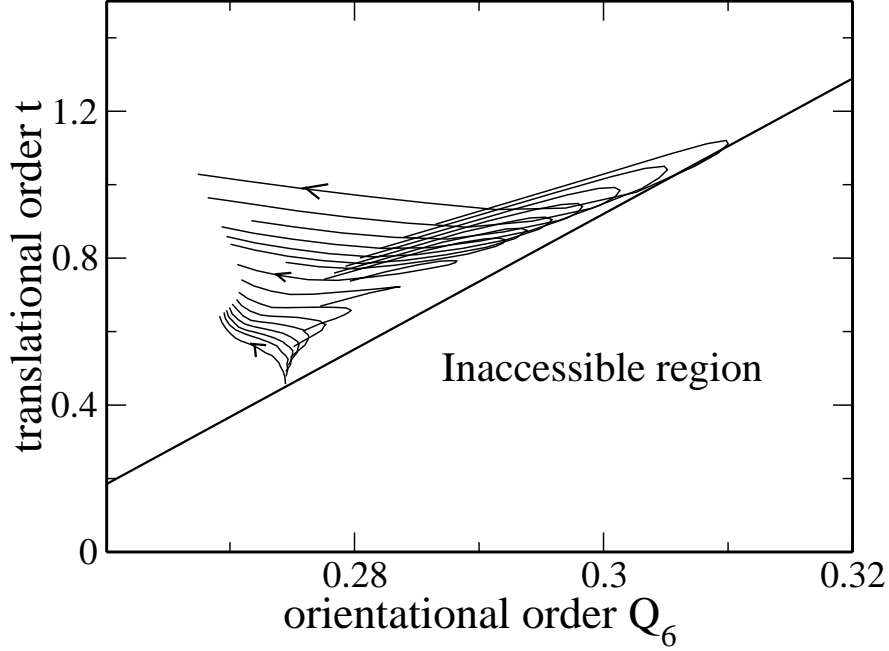


FIG. 8: The $t - Q_6$ plane, or order map. Each line corresponds to an isotherm and the arrows indicate the direction of density growth. From top to bottom, the isotherms showed here are: $T^* = 0.25, 0.3, 0.35, 0.4, 0.45, 0.5, 0.55, 0.7, 1.0, 1.5, 2.0, 2.5, 3.0, 3.5, 4.0$, and 5.0 . Unlike the SPC/E water⁸, the paths formed by the t and Q_6 parameters developed a two dimensional region in the order map for temperatures and densities inside the structural anomalous region. As observed for the SPC/E water⁸.

diagram ordermap collapse into a single line in the structural anomaly region⁸. This property supports the idea that in water the anomalies in translational diffusion and in rotational mobility are related^{3,10,11}.

In order to check if t and Q_6 are also related in our isotropic model, the order map was also constructed. The Fig. 8 shows the behavior of t as a function of Q_6 . The arrows indicate the growth of density for each isotherm. Similar to the results found for the SPC/E water⁸, Silica¹³, and for the ramp potential^{40,41}, was observed an inaccessible region for the order map of our model. However, differently from the SPC/E water⁸, and similarly to the ramp potential^{40,41}, the parameters t and Q_6 do not fall into a straight line in the order map for densities and temperatures inside the region of structural anomalies (note in the Fig. 8 that t and Q_6 develop a two dimensional region in the order map).

V. CONCLUSIONS

Using molecular dynamic simulations we have studied the structure of fluids interacting via a three-dimensional continuous core-softened potential with a continuous force. The translational (t) and orientational (Q_6) order parameters introduced by Steinhardt *el. al.*¹⁸ were analyzed in the framework proposed by Yan *el. al.*⁴⁰ to quantify the structure order for an isotropic liquid.

Our model exhibits a region of density anomaly, inside which the density increases as the system is heated at constant pressure, and a region of diffusion anomaly, where the diffusivity decreases with increasing density⁴³. In the pressure-temperature phase diagram, the density anomaly region lies inside the diffusion anomaly one.

Complementary to the thermodynamic and dynamic anomalies, both t and Q_6 behave anomalously in a large region of the temperature–density plane, as follows. The parameter t have both a local maximum, at a density ρ_{t-max} , and a local minimum at a density $\rho_{t-min} > \rho_{t-max}$. For densities in the range $\rho_{t-max} < \rho < \rho_{t-min}$ the translational order parameter decreases under pressure. For normal liquids the opposite behavior is expected. For the parameter Q_6 , a maximum at a density ρ_{Qmax} between ρ_{t-max} and ρ_{t-min} was observed. Hence, *both* t and Q_6 become anomalous for densities in the range $\rho_{Qmax} < \rho < \rho_{t-min}$. The loci of the Q_6 maxima, t maxima, and t minima were plotted in a temperature–density plane and we showed that the region where t and Q_6 behave anomalously encloses the regions of density and diffusion anomalies discussed above. This is the same behavior observed for the SPC/E water^{8,9}. Differently from SPC/E water, the parameters t and Q_6 do not fall into a straight line in the order map for densities and temperatures what suggests that unlike water t and Q_6 are independent in the anomalous region.

In resume, the studied continuous core-softened pair potential, despite not having long-ranged or directional interactions, exhibits thermodynamic, dynamic⁴³, and structural anomalies similar to the ones observed in SPC/E water^{8,9}. Therefore, we can conclude that the presence of anisotropy in the interaction potential is not a requirement for the presence of thermodynamic, dynamic and structural anomalies.

Acknowledgments

We thank the Brazilian science agencies CNPq, FINEP and Fapergs for financial support.

- ¹ R. Waller, Essays of Natural Experiments, Johnson Reprint corporation, New York , 1964.
- ² <<http://www.lsbu.ac.uk/water/anmlies.html>>.
- ³ P. A. Netz, F. W. Starr, M. C. Barbosa and H. E. Stanley, Physica A **314**, 470 (2002).
- ⁴ F. W. Starr, F. Sciortino and H. E. Stanley, Phys. Rev. E **60**, 6757 (1999); F. W. Starr, S. T. Harrington, F. Sciortino and H. E. Stanley, Phys. Rev. Lett. **82**, 3629 (1999).
- ⁵ P. Gallo, F. Sciortino, P. Tartaglia and S. -H. Chen, Phys. Rev. Lett. **76**, 2730 (1996); F. Sciortino, P. Gallo, P. Tartaglia and S. -H. Chen, Phys. Rev. E **54**, 6331 (1996); S. -H. Chen, P. Gallo, F. Sciortino and P. Tartaglia, *ibid.* **56**, 4231 (1997); F. Sciortino, L. Fabbian, S. -H. Chen and P. Tartaglia *ibid.* **56**, 5397 (1997).
- ⁶ S. Harrington, P. H. Poole, F. Sciortino and H. E. Stanley, J. Chem. Phys. **107**, 7443 (1997).
- ⁷ F. Sciortino, A. Geiger and H. E. Stanley, Nature (London) **354**, 218 (1991); J. Chem Phys. **96**, 3857 (1992).
- ⁸ J. R. Errington and P. G. Debenedetti, Nature (London) **409**, 318 (2001).
- ⁹ P. A. Netz, F. W. Starr, H. E. Stanley and M. C. Barbosa, J. Chem. Phys. **115**, 344 (2001).
- ¹⁰ H. E. Stanley, M. C. Barbosa, S. Mossa, P. A. Netz, F. Sciortino, F. W. Starr and M. Yamada, Physica A **315**, 281 (2002).
- ¹¹ P. A. Netz, F.W. Starr, M. C. Barbosa and H. E. Stanley, J. Mol. Liquids **101**, 159 (2002).
- ¹² C. A. Angell, R. D. Bressel, M. Hemmatti, E. J. Sare, and J. C. Tucker, Phys. Chem. Chem. Phys. **2**, 1559 (2000).
- ¹³ M. S. Shell, P. G. Debenedetti, and A. Z. Panagiotopoulos, Phys. Rev. E **66**, 011202 (2002).
- ¹⁴ P. T. Cummings and G. Stell, Mol. Phys. **43**, 1267 (1981).
- ¹⁵ M. Togaya, Phys. Rev. Lett. **79**, 2474 (1997).
- ¹⁶ J. R. Errington, P. G. Debenedetti, and S. Torquato, J. Chem. Phys. **118**, 2256 (2003).
- ¹⁷ P. L. Chau and A. J. Hardwick, Mol. Phys. **93**, 511 (1998).
- ¹⁸ P. J. Steinhardt, D. R. Nelson, and M. Ronchetti, Phys. Rev. B **28**, 784 (1983).
- ¹⁹ S. Torquato, T. M. Truskett, and P. G. Debenedetti, Phys. Rev. Lett. **84**, 2064 (2000).

- ²⁰ B. Guillot, J. Mol. Liquids **101**, 219 (2002).
- ²¹ For a recent review, see P. Debenedetti, J. Phys.: Condens. Matter **15**, R1669 (2003).
- ²² M. R. Sadr-Lahijany, A. Scala, S. V. Buldyrev, and H. E. Stanley, Phys. Rev. Lett. **81**, 4895 (1998); M. R. Sadr-Lahijany, A. Scala, S. V. Buldyrev, and H. E. Stanley, Phys. Rev. E **60**, 6714 (1999).
- ²³ A. Scala, M. R. Sadr-Lahijany, N. Giovambattista, S. V. Buldyrev and H. E. Stanley, J. Stat. Phys. **100**, 97 (2000); A. Scala, M. R. Sadr-Lahijany, N. Giovambattista, S. V. Buldyrev and H. E. Stanley, Phys. Rev. E **63**, 041202 (2001).
- ²⁴ G. Franzese, G. Malescio, A. Skibinsky, S. V. Buldyrev and H. E. Stanley, Nature **409**, 692 (2001).
- ²⁵ S. V. Buldyrev, G. Franzese, N. Giovambattista, G. Malescio, M. R. Sadr-Lahijany, A. Scala, A. Skibinsky, H. E. Stanley, Physica A **304**, 23 (2002).
- ²⁶ S. V. Buldyrev and H. E. Stanley, Physica A **330**, 124 (2003).
- ²⁷ G. Franzese, G. Malescio, A. Skibinsky, S. V. Buldyrev and H. E. Stanley, Phys. Rev. E **66**, 051206 (2002).
- ²⁸ Aline Balladares and Marcia C. Barbosa, J. Phys.: Cond. Matt. **16**, 8811 (2004).
- ²⁹ Alan B. de Oliveira and Marcia C. Barbosa, J. Phys.: Cond. Matt. **17**, 399 (2005).
- ³⁰ V. B. Henriques and M. C. Barbosa, Phys. Rev. E **71**, 031504 (2005); V. B. Henriques, Nara Guissoni, Marco A. Barbosa, Marcelo Thielo and Marcia C. Barbosa, Mol. Phys. **103**, 3001 (2005).
- ³¹ A. Skibinsky, S. V. Buldyrev, G. Franzese, G. Malescio and H. E. Stanley, Phys. Rev. E **69**, 061206 (2004).
- ³² G. Malescio, G. Franzese, A. Skibinsky, S. V. Buldyrev and H. E. Stanley, Phys. Rev. E **71**, 061504 (2005).
- ³³ P. J. Camp, Phys. Rev. E. **68**, 061506 (2003).
- ³⁴ P. J. Camp, Phys. Rev. E. **71**, 031507 (2005).
- ³⁵ P. C. Hemmer and G. Stell, Phys. Rev. Lett. **24**, 1284 (1970); G. Stell and P. C. Hemmer, J. Chem. Phys. **56**, 4274 (1972); J. M. Kincaid, G. Stell, and C. K. Hall, *ibid.* **65**, 2161 (1976); J. M. Kincaid, G. Stell, and E. Goldmark, *ibid.* **65**, 2172 (1976); C. K. Hall and G. Stell, Phys Rev. A **7**, 1679 (1973); E. Velasco, L. Medeiros, G. Navascués, P. C. Hemmer and G. Stell, Phys. Rev. Lett. **85**, 122 (2000); P. C. Hemmer, E. Velasco, L. Mederos, G. Navascués and G.

- Stell, J. Chem. Phys. **114**, 2268 (2001).
- ³⁶ E. A. Jagla, Phys. Rev. E **58**, 1478 (1998); E. A. Jagla, J. Chem. Phys. **110**, 451 (1999); E. A. Jagla, J. Chem. Phys. **111**, 8980 (1999); E. A. Jagla, Phys. Rev. E **63**, 061501 (2001); E. A. Jagla, Phys. Rev. E **63**, 061509 (2001).
- ³⁷ N. B. Wilding and J. E. Magee, Phys. Rev. E **66**, 031509 (2002).
- ³⁸ P. Kumar, S. V. Buldyrev, F. Sciortino, E. Zaccarelli and H. E. Stanley, Phys. Rev. E **72**, 021501 (2005).
- ³⁹ L. Xu, P. Kumar, S. V. Buldyrev, S.-H. Chen, P. H. Poole, F. Sciortino, and H. E. Stanley, Proc. Natl. Acad. Sci. U.S.A. **102**, 16558 (2005).
- ⁴⁰ Z. Yan, S. V. Buldyrev, N. Giovambattista, and H. E. Stanley, Phys. Rev. Lett. **95**, 130604 (2005).
- ⁴¹ Z. Yan, S. V. Buldyrev, N. Giovambattista, P. G. Debenedetti, and H. E. Stanley, Phys. Rev. E **73**, 051204 (2006).
- ⁴² H. M. Gibson and N. B. Wilding, Phys. Rev. E **73**, 061507 (2006).
- ⁴³ A. B. de Oliveira, P. A. Netz, T. Colla, and M. C. Barbosa, J. Chem. Phys. **124**, 084505 (2006).
- ⁴⁴ C. H. Cho, S. Singh and G. W. Robinson, Phys. Rev. Lett. **76**, 1651 (1996); Faraday Discuss. **103**, 19 (1996); J. Chem. Phys. **107**, 7979 (1997).
- ⁴⁵ C. H. Cho, S. Singh, and G. W. Robinson. Phys. Rev. Lett. **79**, 180 (1997).
- ⁴⁶ Paulo A. Netz, J. Fernando Raymundi, Adriana Simone Camera and Marcia C. Barbosa, Physica A **342**, 48 (2004).
- ⁴⁷ This cut-off was choosen inspired in the Refs.^{40,41}. An alternative might have been the distance corresponding to the first or second minimum in g . These different options do not affect the location of ρ_{t-max} and ρ_{t-min} .
- ⁴⁸ T. M. Truskett, S. Torquato, and P. G. Debenedetti, Phys. Rev. E **62**, 993 (2000).
- ⁴⁹ A. Huerta, G. G. Naumis, D. T. Wasan, D. J. Henderson, and A. D. Trokhymchuk, J. Chem Phys. **120**, 1506 (2004).
- ⁵⁰ In Refs.^{16,19,48,49} the average of Y_{lm} is taken over *all* bonds in the system. Therefore, no 'local order' concept exists. On the other hand, in Refs.^{8,13} the average of Y_{lm} is taken over the four nearest neighbors, quantifying a tetrahedral local order for the system. The orientational order parameter of this work is based on the idea of local order for each particle, similar to Refs.^{8,13}.
- ⁵¹ We have tested the use of a larger cutoff (5.5σ) and it does not affect the results.

⁵² W. G. Hoover, Phys. Rev. A **31**, 1695 (1985); *ibid* **34**, 2499 (1986).

⁵³ This new peak may be interpreted as a signal of clustering. In order to check this, some snapshots for $T^* = 0.25$ and the range of densities spanned by the Fig. 5 were taken. These snapshots (not shown) even displaying a non-random distribution of particles, do not show clearly any clustering.